JGR Atmospheres

RESEARCH ARTICLE
10.1029/2019JD031685

Exploring Oxidation in the Remote Free Troposphere: Insights From Atmospheric Tomography (ATom)

W. H. Brune[1], D. O. Miller[1], A. B. Thames[1], H. M. Allen[2], E. C. Apel[3], D. R. Blake[4], T. P. Bui[5], R. Commane[6], J. D. Crounse[2], B. C. Daube[7], G. S. Diskin[8], J. P. DiGangi[8], J. W. Elkins[9], S. R. Hall[3], T. F. Hanisco[10], R. A. Hannun[11,10], E. J. Hintsa[12,9], R. S. Hornbrook[3], M. J. Kim[13], K. McKain[12,9], F. L. Moore[12,9], J. A. Neuman[14,12], J. M. Nicely[15,10], J. Peischl[12,14], T. B. Ryerson[14], J. M. St. Clair[11,10], C. Sweeney[9], A. P. Teng[13,16], C. Thompson[17,12,14], K. Ullmann[3], P. R. Veres[14], P. O. Wennberg[13], and G. M. Wolfe[11,10]

[1]Department of Meteorology and Atmospheric Science, Pennsylvania State University, University Park, PA, USA, [2]Division of Chemistry and Chemical Engineering, California Institute of Technology, Pasadena, CA, USA, [3]Atmospheric Chemistry Observations and Modeling Laboratory, National Center for Atmospheric Research, Boulder, CO, USA, [4]Department of Chemistry, University of California, Irvine, CA, USA, [5]Earth Science Division, NASA Ames Research Center, Moffett Field, CA, USA, [6]Department of Earth and Environmental Sciences of Lamont-Doherty Earth Observatory, Columbia University, Palisades, NY, USA, [7]Department of Earth and Planetary Sciences, Harvard University, Cambridge, MA, USA, [8]Chemistry and Dynamics Branch, NASA Langley Research Center, Hampton, VA, USA, [9]Global Monitoring Division, Earth System Research Laboratory, NOAA, Boulder, CO, USA, [10]Atmospheric Chemistry and Dynamics Laboratory, NASA Goddard Space Flight Center, Greenbelt, MD, USA, [11]Joint Center for Earth Systems Technology, University of Maryland, Baltimore County, Baltimore, MD, USA, [12]Cooperative Institute for Research in Environmental Sciences, University of Colorado Boulder, Boulder, CO, USA, [13]Division of Geological and Planetary Sciences, California Institute of Technology, Pasadena, CA, USA, [14]Chemical Sciences Division, Earth System Research Laboratory, NOAA, Boulder, CO, USA, [15]Earth System Science Interdisciplinary Center, University of Maryland, College Park, MD, USA, [16]Now with Divergent 3D, Los Angeles, CA, USA, [17]Now with Scientific Aviation, Boulder, CO, USA

Abstract Earth's atmosphere oxidizes the greenhouse gas methane and other gases, thus determining their lifetimes and oxidation products. Much of this oxidation occurs in the remote, relatively clean free troposphere above the planetary boundary layer, where the oxidation chemistry is thought to be much simpler and better understood than it is in urban regions or forests. The NASA airborne Atmospheric Tomography study (ATom) was designed to produce cross sections of the detailed atmospheric composition in the remote atmosphere over the Pacific and Atlantic Oceans during four seasons. As part of the extensive ATom data set, measurements of the atmosphere's primary oxidant, hydroxyl (OH), and hydroperoxyl (HO_2) are compared to a photochemical box model to test the oxidation chemistry. Generally, observed and modeled median OH and HO_2 agree to within combined uncertainties at the 2σ confidence level, which is ~$\pm$40%. For some seasons, this agreement is within ~$\pm$20% below 6-km altitude. While this test finds no significant differences, OH observations increasingly exceeded modeled values at altitudes above 8 km, becoming ~35% greater, which is near the combined uncertainties. Measurement uncertainty and possible unknown measurement errors complicate tests for unknown chemistry or incorrect reaction rate coefficients that would substantially affect the OH and HO_2 abundances. Future analysis of detailed comparisons may yield additional discrepancies that are masked in the median values.

Plain Language Summary Chemistry in the vast, remote atmosphere destroys methane and other greenhouse gases. This chemistry is thought to be simple and well understood compared to that in polluted cities or in forests. From the NASA airborne Atmospheric Tomography study over remote oceans, comparisons of observed and modeled reactive gases show that the chemistry is generally understood to within the uncertainties of the measurement and model. However, for the atmosphere's primary reactive gas, hydroxyl, measured values exceed modeled values in the upper troposphere, pointing to errors in probably the measurements but possibly the model chemistry.

Key Points:
- Free tropospheric hydroxyl and hydroperoxyl radical chemistry appears to be understood to within measurement and model uncertainty of ±40%
- Observed hydroxyl often exceeded modeled values in the upper troposphere, but measurement uncertainty masks any model chemistry errors
- A hydroxyl measurement interference found in forests for this instrument does not exist throughout the free troposphere, even near convection

Supporting Information:
- Supporting Information S1

Correspondence to:
W. H. Brune,
whb2@psu.edu

Citation:
Brune, W. H., Miller, D. O., Thames, A. B., Allen, H. M., Apel, E. C., Blake, D. R., et al. (2020). Exploring oxidation in the remote free troposphere: Insights from Atmospheric Tomography (ATom). *Journal of Geophysical Research: Atmospheres*, *125*, e2019JD031685. https://doi.org/10.1029/2019JD031685

Received 17 SEP 2019
Accepted 19 DEC 2019
Accepted article online 27 DEC 2019

1. Introduction

Oxidation in the atmosphere determines the lifetimes and fates of the greenhouse gas methane (CH_4), thousands of volatile organic compounds (VOCs), sulfur compounds, and gaseous emissions from combustion. On a global scale, the hydroxyl radical (OH) drives atmospheric oxidation. OH is chemically coupled to the hydroperoxyl radical (HO_2), which is responsible in large part for ozone (O_3) production in polluted conditions and O_3 removal in clean conditions. The remote atmosphere over oceans is predominantly relatively clean, with pollution plumes passing through depending on the location and season. Because most of the atmosphere is over oceans, most of the atmospheric oxidation occurs there. Thus, a solid understanding of OH chemistry for the remote atmosphere is critical for developing predictive capability for the atmospheric oxidation potential and for climate change.

OH comes primarily from the photolysis of ozone (O_3) that produces an excited state oxygen atom ($O(^1D)$), which reacts with water vapor (H_2O) to make two OH molecules. Other important sources are photolysis of hydrogen peroxide (HOOH), methyl hydroperoxide (CH_3OOH), and peroxyacetic acid (CH_3CO_3H) to make OH and photolysis of formaldehyde (HCHO) and acetaldehyde (CH_3CHO) to make HO_2. OH reacts with thousands of atmospheric constituents, but, for the global atmosphere, the most important of these are carbon monoxide (CO), methane (CH_4), methane's oxidation products such as HCHO, and nitrogen oxides ($NO_x = NO + NO_2$). In regions with sufficient NO_x, NO reacts with HO_2 to form OH and NO_2, which leads to O_3 formation, while NO_2 reacts with OH to make nitric acid (HNO_3), causing the loss of the sum of HO_2 and OH, called HO_x. In the cleaner tropospheric regions, where NO_x is less than a few tens of parts per trillion by volume (pptv), reactions of HO_2 with OH, HO_2, and methyl peroxyl (CH_3O_2), a CH_4 oxidation product, cause much of the HO_x loss. While tropospheric VOC oxidation still has many unknowns in reaction pathways, rates, and mechanisms, the chemistry of CO, CH_4, and minimal NO_x in the remote troposphere is thought to be fairly well understood.

A typical midlatitude surface concentration of OH was first calculated with a rather simple photochemical model for unpolluted conditions in the lower troposphere (Levy, 1971). His calculation assumed that the primary OH source was $O(^1D) + H_2O$ and that NO_x abundances were equivalent to 3 ppbv. Calculated midday values in the lower troposphere were 3.7×10^6 cm^{-3} (0.15 pptv) for OH and 5×10^8 cm^{-3} (20 pptv) for HO_2. Logan et al. (1981) used a more detailed two-dimensional model to calculate the global meridional mean OH as a function of altitude and latitude. From this model, the calculated midday OH concentration was greatest (~7×10^6 cm^{-3}) in the lower tropics and decreased by about a factor of 3 vertically at 14-km altitude and horizontally at about $\pm 60^\circ$ latitude. The calculated HO_2 concentrations fell off from their peak values in the lower tropics (8×10^8 cm^{-3}) by about a factor of 10 over the same ranges. For the midlatitudes just above Earth's surface, these two calculations for OH and HO_2 agree to within a factor of 1.5.

The degree of understanding of atmospheric oxidation can be tested by comparing observed OH and HO_2 to calculated values from a photochemical box model that is constrained with simultaneous measurements of environmental conditions and chemical constituents. This approach works for OH and HO_2 because their lifetimes are a fraction of a second for OH and tens of seconds for HO_2. However, until the mid-1990s, airborne instruments could not measure tropospheric OH and/or HO_2.

In late 1995, an instrument on the NSF C-130 aircraft measured OH in the remote atmosphere at altitudes between 0 and 6 km over the Pacific Ocean near Tasmania, Australia (Mauldin et al., 1998). The scatterplot of the observed OH as a function of OH modeled with a photochemical box model had a slope of 0.97 and an R^2 of 0.68, although the study had no direct photolysis frequency measurements, which are important in the presence of clouds. For the first airborne tropospheric measurements, this agreement is remarkable.

About the same time, an instrument on the NASA ER-2 aircraft measured OH in the remote upper troposphere, between 7- and 16-km altitude, near Hawaii (Wennberg et al., 1998). While the observed cycling between OH and HO_2 agreed to within a factor of 1.3 with the modeled cycling, observed OH was about twice modeled OH. Acetone photolysis was proposed as the missing OH source, but the photolysis frequencies are now known to be much too small at upper tropospheric temperatures for this source to be important (Blitz et al., 2004). Shortly after, airborne measurements of OH and HO_2 with a different instrument also found that observed OH and HO_2 exceeded modeled by a factor of 2 at altitudes from 7 to 12 km (Brune

et al., 1998; Jaeglé et al., 1998; Jaeglé et al., 2000). In both of these studies, HCHO, HOOH, and other oxygenated volatile organic compounds (OVOCs), which were not measured, could be the likely missing HO_x sources in the models.

Subsequent airborne studies in the remote troposphere have produced a range of agreement between observed and modeled OH and HO_2 (Table S1; for a review, see Stone, Whalley, & Heard, 2014). These observations were made by either Laser-Induced Fluorescence (LIF; Faloona et al., 2004; Martinez et al., 2010) or by Chemical Ionization Mass Spectrometry (CIMS; Mauldin et al., 1999; Cantrell et al., 2003a). Some of these studies were primarily in air influenced by upwind land pollution (Brune et al., 2018; Cantrell et al., 2003b; Martinez et al., 2010; Olson et al., 2004; Stone, Evans, Commane, et al., 2010; Stone, Evans, Edwards, et al., 2011; Regelin et al., 2013; Stone, Evans, Walker, 2014; Ren et al., 2008; Tan et al., 1998). Others were in relatively clean air, either at high latitudes (Cantrell, Mauldin, et al., 2003; Olson et al., 2012; Ren et al., 2012) or the remote Pacific Ocean (Adhikary et al., 2010; Chen et al., 2001; Mao et al., 2010; Mauldin et al., 1998; Mauldin et al., 1999; Davis et al., 2001; Mauldin et al., 2001; Tan et al., 2001). For most of these studies, observed and modeled OH generally agreed to within uncertainties, which were approximately $\pm$(30–40)% (2σ confidence) for both observations and models. In some of the earlier studies, the models were not well constrained by critical measurements, but for later studies with constraints from more measurements, the same levels of agreement were often seen.

There are some notable exceptions. First, for LIF in INTEX-A, flights over the eastern United States, observed HO_2 and the HO_2/OH ratio agree with modeled values below 8 km but were 1.5–3.0 times modeled values above 8-km altitude (Ren et al., 2008). Second, for TRACE-P over the eastern North Pacific, OH observed by LIF and CIMS were 1.4–1.5 times the modeled values below 2 km, while at higher altitudes, OH by LIF was equal to the model to within 20% from 5 to 11 km and OH by CIMS was 0.7 times the modeled value at 6 km (Olson et al., 2004). HO_2 observed by LIF was generally 1.32 times modeled at all altitudes, but was 2.6 times modeled in air from the lowermost stratosphere. Note that the LIF TRACE-P measurements in Olson et al. (2004) require a correction of 1.64 (Ren et al., 2008). Third, for ARCTAS in the Arctic spring, OH measured by CIMS agreed with the model up to 6 km, but then decreased monotonically to ~20% of the model at 10 km, although the median OH observed by LIF agreed with the model to within 10% for 0–12 km while HO_2 observed by LIF was only 0.6 of modeled for all altitudes (Ren et al., 2012). In the summer phase of ARCTAS, both OH and HO_2 by LIF had a decreasing trend in the observed-to-modeled ratio with altitude—for OH, going from 1.4 at the surface to 0.9 above 8 km and, for HO_2, going from 1.3 at the surface to 0.6 above 8 km (Olson et al., 2012). These discrepancies, which have little in common, are all larger than expected from the estimated uncertainties in the measurements and models. They have not been resolved and provide a caution to the generally good agreement to within uncertainties found for the other missions.

To test the understanding of global tropospheric oxidation, all of the existing missions that covered different global regions could be combined to increase the coverage of measurements in the remote atmosphere over oceans. However, this approach has a problem: the unknown consistency of the instruments and models used in the missions. Any variation in agreement between observed and modeled OH and HO_2 could be due to differences in the HO_x instrument or instrument performance, model chemistry, or the presence or quality of the simultaneous measurements of other chemical species or environmental factors that are used to constrain the model.

The Atmospheric Tomography (ATom) study overcomes this problem by using the same instruments and models to examine the oxidation chemistry of the remote free troposphere from northern high latitudes to southern high latitudes 4 times, once in each season, over the course of approximately two years. The NASA DC-8 carried an instrument suite capable of measuring OH and HO_2, more than 100 other chemical species, many photolysis frequencies, and environmental parameters. No previous study has covered so much of the troposphere with such a comprehensive measurement suite and for all four seasons.

By comparing the observed OH and HO_2 to that calculated with a photochemical box model constrained by the other measurements, we expect to demonstrate that the rather simple oxidation chemistry for OH and HO_2 in the clean, remote free troposphere is well understood over the wide range of environmental conditions encountered in ATom. This paper presents an overview of the comparisons of observed and modeled OH and HO_2 in the free troposphere.

2. Methods

2.1. ATom

The goal of ATom was to sample the typical global atmospheric composition to provide observations that can be used to test and improve global chemical transport models and climate models. Unlike most previous missions, there were no deviations from the flight paths to sample pollution plumes or unusual meteorological conditions. The NASA DC-8 flew essentially the same route 4 times (Figure 1).

Each ATom phase started with a flight to the equator and back from the NASA DC-8 base in Palmdale, CA, followed by flights to Anchorage, AK., Kona, HI; Pago Pago, American Somoa or Nadi, Fiji; Christchurch, New Zealand; Punta Arenas, Chile; Ascension Island or Recife, Brazil; Terceira-Azores, Portugal; Greenland; Anchorage, AK; and back to Palmdale, CA, with some minor deviations in each mission. The dates of each phase were chosen to sample the remote atmosphere once in each season: ATom-1, 28 July to 22 August 2016; ATom-2, 26 January to 22 February 2017; ATom-3, 28 September to 26 October 2017; and ATom-4, 24 April to 21 May 2018. Each flight consisted of ascent to the highest altitude possible, typically 10 to 13 km, remain there for 5 min, descent to 150 m, remain there for 5 min, and ascent to the highest altitude. This pattern was repeated as often as possible during each flight, typically 6–9 times. This approach provided global maps of detailed atmospheric composition.

2.2. DC-8 Measurements

Simultaneous measurements of photolysis frequencies, environmental state variables, aerosol properties, and chemical species were made by different research groups on the NASA DC-8. The measurements used in the analysis here are listed in Table S2. The primary use of these data was to constrain the photochemical box model. For details of these other instruments and measurements, please see Table S2 and the references therein.

2.3. Measurements of OH and HO_2

OH and HO_2 were both measured using the Penn State Airborne Tropospheric Hydrogen Oxides Sensor (ATHOS) instrument (Faloona et al., 2004). ATHOS uses the fluorescent assay by gas expansion technique developed by Hard et al. (1984) and Stevens et al. (1994). The laser, detection cells, and electronics sit in the forward cargo bay, and the sampling tube extends down into a large nacelle that is used to slow the airflow to ~10 m s^{-1} at the sampling inlet, which is perpendicular to the flow. Sample air is drawn into the instrument through an inlet (1.3-mm diameter) where it enters a low-pressure environment. The air travels for ~22 ms along a flow tube to the two detection axes. In each detection axis, the 308-nm laser beam (3-kHz repetition rate, 20-ns pulses) crosses the sample air stream 32 times where it is absorbed by OH, resulting in fluorescence. Between the two axes, reagent nitric oxide (NO) is introduced into the sample air stream where it converts HO_2 to OH, which is detected in the second axis. The resulting fluorescence signals are measured by microchannel plate detectors. The laser wavelength is tuned on-resonance (online) and off-resonance (off-line) with the OH fluorescence signal being the difference between the online and off-line signals. The online/off-line times were 15/15 s for ATom-1, 10/10 s for ATom-2 and ATom-3, and 20/10 s for ATom-4.

In regions with substantial levels of alkenes and aromatics, ATHOS has been shown to have an interference (Feiner et al., 2016; Mao et al., 2012). To mitigate the potential interferences for ATom, a second method of OH detection was also used. An OH reactant, perfluoropropylene (C_3F_6), was added upstream of the detection inlet in order to scavenge all the ambient OH before it enters the inlet. To control the reactant addition, a small cylinder with an aerodynamic outer shell was placed over the inlet. Four small injectors ringed the inside of the cylinder 3.0 cm upstream of the inlet. The C_3F_6 flow of 0.9 sccm for ATom-1 and 1.3 sccm for ATom -2, -3, and -4 was added to a 70-sccm N_2 flow in a chamber inside the cylinder walls, which pushed the C_3F_6 through the injectors in order to improve mixing with the ambient air in the cylinder.

Ambient air was pushed through the cylinder by ram force. The flow in the cylinder was slowed by a disk with holes set at the end of the cylinder, giving a typical reaction time of ~2 ms and fractional ambient OH removed of 82±5% for ATom-1 and 91±5% for ATom-2, -3, and -4, 2σ confidence. The reactant was added for 1 min in a 2-min cycle. The measured OH is the difference in the OH measured without reactant and with reactant, corrected for the incomplete external removal and the small internal removal (<5%). The remainder is the OH interference. More details about this method are given in the supporting information.

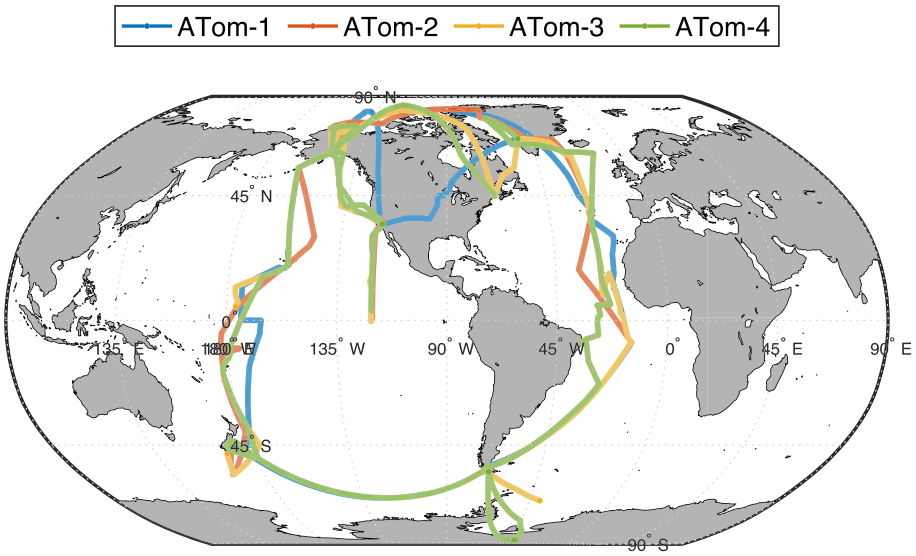

Figure 1. Map of ATom flight routes.

Measuring HO_2 by adding reagent NO to convert all the HO_2 to OH has been shown to have an interference from the peroxy radicals that come from larger aromatic, alkene, and cycloalkane chemicals (Feiner et al., 2016; Fuchs et al., 2011; Whalley et al., 2013). This interference becomes negligible when the added NO is only enough to convert less than 30% of the HO_2 to OH in a few milliseconds. For ATom, the NO flow of 0.5 sccm converted 28% of the HO_2. Every sixth laser online/off-line cycle, 7 sccm of NO was added, which is enough to convert all the HO_2 to OH and thus provides a test of the presence of the organic peroxy radicals from these larger aromatics, alkenes, and cycloalkanes.

The ATHOS instrument is calibrated in the laboratory before and after each ATom deployment and, on two occasions, in the hangar on the aircraft before deployment. The calibrations for OH and HO_2 are functions of the detection cell pressure, which is proportional to the atmospheric pressure. The detection cell pressures were changed by using different inlet sizes, a method that has been shown to agree well with a more complicated method that does not require changing the inlet diameter (Stone, Whalley, & Heard, 2014). Details about the calibration procedure can be found in Faloona et al. (2004). For OH detection using the scavenger method and for HO_2 detection using only partial conversion, the estimated absolute uncertainty for ATom is $\pm$35%, 2σ confidence, for both OH and HO_2.

The limit of detection (LOD) is set for OH by counting statistics and for HO_2 by small impurities that could not be removed from the reagent NO. For 1-min averages measured in the dark on ATom flights, the standard deviation is 0.018 pptv for OH and 0.2 pptv for HO_2. This standard deviation is taken to be the LOD. In concentration units, the OH LOD is 4.5×10^5 cm^{-3} at 0-km altitude and 1.5×10^5 cm^{-3} at 10 km for 1-min averages.

2.4. Photochemical Box Model

The Framework for 0-D Atmospheric Modeling (Wolfe et al., 2016) is the photochemical box model framework used to calculate OH and HO_2. This model uses the Master Chemical Mechanism, v3.3.1, for all gas-phase reactions (Jenkin et al., 2003; Saunders et al., 2003). Both the Framework for 0-D Atmospheric Modeling model framework and Master Chemical Mechanism v3.1.1 are publicly available. The standard model for this analysis was augmented with the reactions of CH_3O_2 + OH and $C_2H_5O_2$ + OH, which cycle OH to HO_2, to account for recent laboratory measurements of these rate coefficients (Assaf et al., 2017). The model was run with the integration time set to three days with a decay time for unmeasured OVOCs (called the dilution time) of 12 hr.

The model was constrained by the simultaneous measurements listed in Table S2. These measurements were taken from the 1-s merge file, averaged to 1-min values, and interpolated to a common 1-min time

step. For multiple measurements of a chemical species, a primary measurement was chosen and large gaps were filled with secondary measurements. This method works for the analysis of median comparisons of observed and modeled OH and HO_2.

The model uncertainty can best be determined using global sensitivity analysis, but this tool will take a while to develop for Framework for 0-D Atmospheric Modeling and Master Chemical Mechanism. Global sensitivity analysis involves running the model hundreds to thousands of times, randomly varying all model input chemical species, reaction rate coefficients, and photolysis frequencies within their uncertainty limits each time. Uncertainties for modeled OH and HO_2 are given by the standard deviations of the distributions of the modeled values. For now, we will assume that the model uncertainty is $\pm$20%, 1σ confidence (Chen et al., 2012; Christian et al., 2017; Olson et al., 2012; Thompson & Stewart, 1991).

The model was run several more times to test for sensitivity to model parameters and the photochemical mechanism. First, the model integration time was varied from 6 hr to five days. Second, the model dilution time was varied from half to five days. Third, the uptake of HO_2 and OH on aerosol was added for a few model runs, assuming an uptake coefficient of 0.2 and a loss of HO_x to the aerosol particles. Fourth, the halogen chemical mechanism of Stone et al. (2018) was added to the photochemistry for a few model runs. BrO measurements were made on ATom-3 and ATom-4 and were typically below 0.5 pptv.

The model sensitivity was also found for the uncertainties in the constraining measured chemical species. Three of the most important constraining measurements are NO measured by NOAA NO_yO_3 for OH, and HCHO measured by NASA ISAF, and the oxygenated volatile organic compounds measured by Caltech CIMS (hydrogen peroxide, methyl hydroperoxide, peroxyacetic acid) and by NCAR TOGA (methanol, acetaldehyde, ethanol, acetone, propanal, butanal, acrolein) for both OH and HO_2. These are marked by asterisks in Table S2. Uncertainties at the 2σ confidence level were added or subtracted to the measured NO, HCHO, or OVOC values. The CIMS OVOC uncertainty limits were set by adding $\pm$(30% of the measured values + offsets) to the measured values. Sensitivity tests were run for NO, OVOCs, and CIMS OVOCs one at a time.

2.5. Model Statistics

Several statistical metrics were used to determine the agreement between the observed and modeled OH and HO_2. The slope and intercept of the scatterplots of observed versus modeled OH and HO_2 were found using a York fit, which accounts for uncertainty in both the observations and the measurements (York et al., 2004). Other metrics use the 1-min data for pairwise determination of the R^2, the ratio of observation to model, and the percent difference given in equation (1).

$$PD = 100\times\frac{(observation-model)}{(observation+model)/2} \quad (1)$$

3. Data

The data used in this analysis (Wofsy et al., 2018) are publicly available from the Oak Ridge National Laboratory DAAC (https://doi.org/10.3334/ORNLDAAC/1581). The version used is 1.2.

The data have been filtered to remove periods when OH and HO_2 values are at the instrument limit of detection so that the observed-to-modeled ratio and the percent difference for small values do not vary wildly. The data points used in the following analysis have been filtered for times when OH and HO_2 observed and modeled values all exist, the time is within $\pm$3 hr of local solar noon, the clouds are not thick as determined by the Rayleigh scattering in the OH detection axis, and photolysis and formaldehyde measurements were available. Data are called stratospheric when O_3 was greater than 100 ppbv and have been removed for all analyses of tropospheric OH and HO_2. The sensitivity of the results to these criteria was examined by changing the filter parameters, which resulted in little change of the quantitative relationships between the observed and modeled OH and HO_2 but did decrease the R^2 when filters were relaxed or removed.

The results are organized into latitude bands for analysis. These bands are the following: south polar region (SP), latitude < −60°; southern midlatitudes (SML), −60° < latitude < −20°; tropics (TP), −20° < latitude < 20°; northern midlatitudes (NML), 20° < latitude < 60°; and north polar region (NP), latitude > 60°.

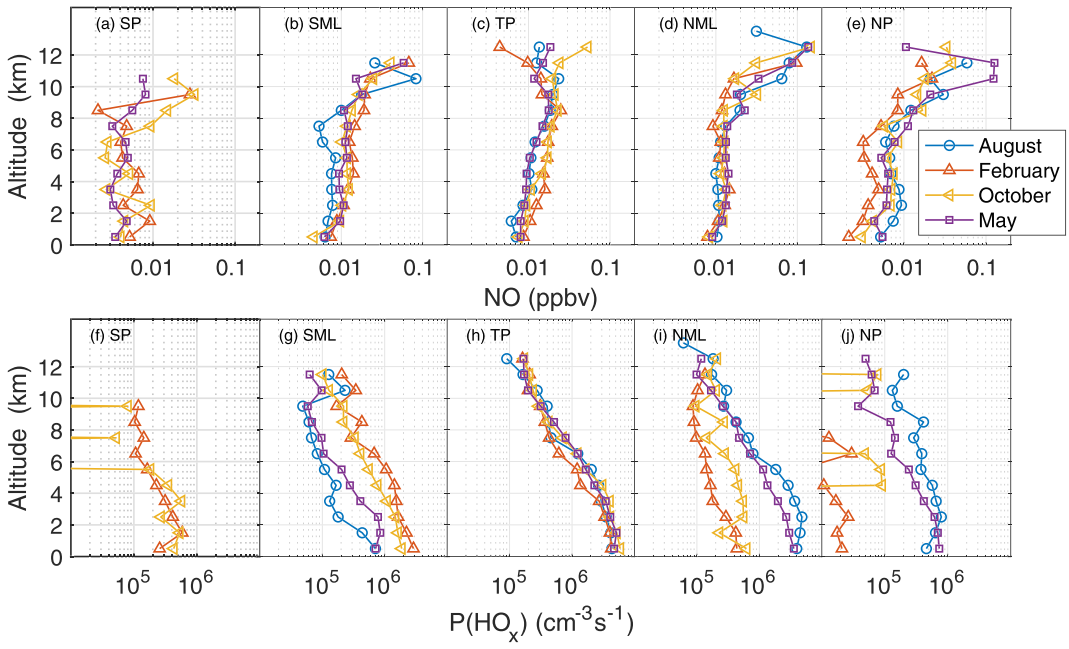

Figure 2. Median altitude profiles of NO and P (HO_x) in five latitude bins for the four ATom periods. Data are filtered as described in the text.

4. Results

4.1. Chemical Species and Factors That Control HO_x

Relatively few chemical species and environmental conditions are thought to control OH and HO_2 over the remote oceans (Figure S2). During ATom, as in some previous campaigns, the production of HO_x (P (HO_x)) was predominantly due to ozone photolysis followed by the reaction of $O(^1D) + H_2O$ at lower altitudes and the photolysis of HCHO at higher altitudes, with comparable contributions from the photolysis of H_2O_2, CH_3CO_3H, and CH_3CHO. Half of the HO_x loss was caused by the reaction $HO_2 + HO_2$ at all altitudes, while $HO_2 + CH_3O_2$ was the second most important HO_x sink at low altitudes and $OH + HO_2$ was the second most important HO_x sink at high altitudes. Note that the $HO_2 + HO_2$ loss, which produces H_2O_2, is 2–5 times greater than the H_2O_2 + hv production of OH so that $HO_2 + HO_2$ is a net sink of HO_x.

The air sampled in ATom was relatively clean, with only infrequent encounters with recent biomass burning or industrial pollution (Figure 2). NO was typically less than a few tens of pptv, being lowest in the polar regions where the solar radiation was weakest, and greatest in the upper mid-to-high-latitude troposphere where stratospheric and tropospheric air mix. P (HO_x) was greatest in the tropics with no seasonal dependence, lowest in the polar regions, and strongly seasonally dependent in the mid-to-high latitudes. Note the expected seasonal flipping of P (HO_x) in the midlatitudes and polar regions. Thus, ATom provided an excellent test of oxidation chemistry involving OH and HO_2 in the relatively clean remote atmosphere.

4.2. OH and HO_2 Measurements as a Function of Altitude and Latitude

Median midday OH was less than 5×10^6 cm^{-3} throughout the troposphere for all seasons, although OH 1-min measurements exceeded 1×10^7 cm^{-3} at times in the planetary boundary layer. In the tropics, median OH was ~4.5×10^6 cm^{-3} in the lower troposphere and decreased to ~2×10^6 cm^{-3} in the upper troposphere for all four seasons (Figures 3a–3e). Further from the tropics, median OH shows the expected strong dependence on season due mainly to its dependence on P (HO_x).

The OH percent difference between observations and models (equation (1)) is within the −40% to +40% combined measurement and model uncertainties 63% of the time for ATom-1, 68% of the time for ATom-2, 80% of the time for ATom-3, and 77% of the time for ATom-4, indicating some possible statistically

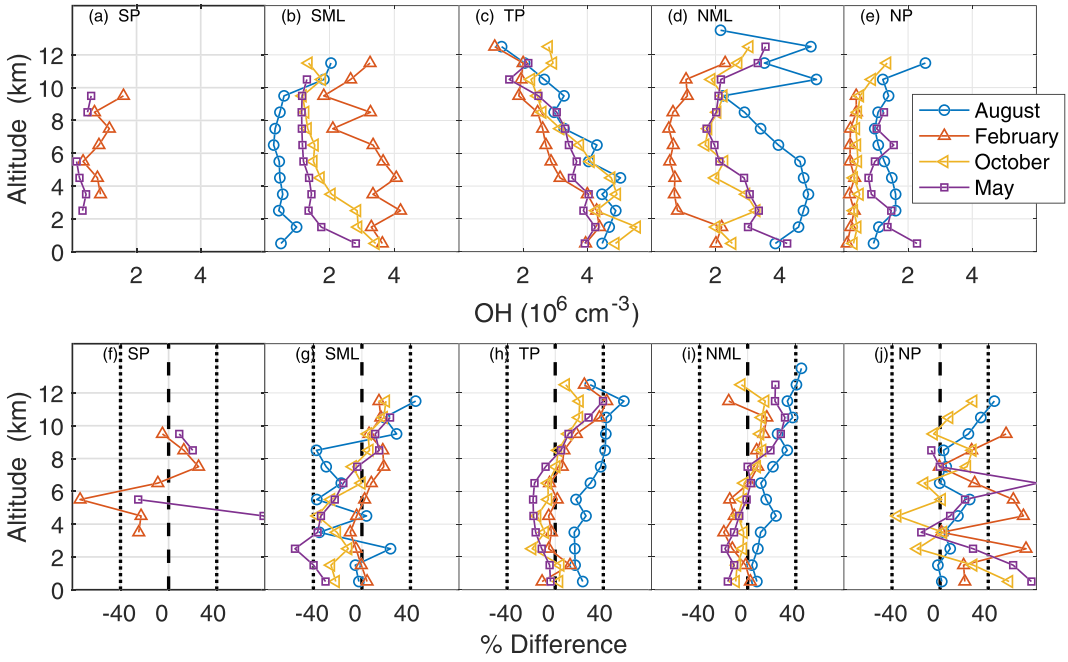

Figure 3. (a–e) Median midday altitude profiles of OH and (f–j) the percent difference (equation (1)) between observed and modeled OH in five latitude bins for the four ATom periods (Table 1). Vertical dotted lines (f–j) indicate uncertainty (2σ confidence) in the percent difference due to model and measurement uncertainty.

significant difference between the observed and modeled OH, especially for ATom-1 (Figures 3f–3j and Table 1). The greatest scatter in the percent difference is in the polar regions, but this variation is not surprising given the OH concentrations are in some cases well below 10^6 cm^{-3}, close to the ATHOS LOD.

Median midday HO_2 is less than 30 pptv throughout the troposphere for all seasons and altitude bands (Figures 4a–4e). Similar to OH, HO_2 is relatively constant and greatest in the tropics and shows the expected seasonal dependence in mid-to-high altitudes. The midlatitude seasonal variation of HO_2 is consistent with the square root of P (HO_x), as expected from theory. For example, in the northern midlatitudes at 6 km, P (HO_x) changes by a factor of 10 between August and February while HO_2 changes a factor of 3.2 from 6 to 19 pptv.

The HO_2 percent difference is within the −40% to 40% band more than 83% of the time for all ATom phases, indicating no significant difference between the observed and modeled HO_2 (Figures 4f–4j). However, for the tropics and northern midlatitudes, the percent difference is slightly positive in the lower troposphere, slightly negative in the middle troposphere, and, on average, is about as positive in the upper troposphere as it is in the lower troposphere.

The relationship between observed and modeled OH and HO_2 can be tested using different statistical tests (Table 1). The slopes of linear fits of the scatterplots of observed versus modeled OH vary from 1.12 for May (ATom-4) to 1.36 for August (ATom-1) and median ratios are 1.01–1.28. The median percent differences are (1.2–25.0)%, with August exhibiting the worst agreement and May (ATom-4) exhibiting the best, with the largest percent differences occurring in the upper troposphere. The slopes of linear fits of the scatterplots of observed versus modeled HO_2 vary from 0.95 for February to 1.19 for August. The median ratios are in the range 0.86 and 1.11. The median percent differences are (−14.8–10.4). For both OH and HO_2, (68–94)% of the variance is captured by the model. These statistical tests indicate that observed and modeled OH and HO_2 agree as well for ATom as they do for any previous airborne field campaigns, although ATom-1 agreement is marginal. However, as is seen in altitude trends for OH and HO_2 percent differences, these statistical tests do not tell the whole story.

The HO_2/OH ratio is often used as a test of HO_x cycling between OH and HO_2 because the cycling rates are so much greater than the HO_x production and loss rates. For ATom, this condition is not valid because of the

Table 1
Statistical Properties: Observed and Modeled OH and HO_2

OH or HO_2	Property	ATom-1	ATom-2	ATom-3	ATom-4
	No. of filtered 1-min data points	2642	2211	1799	3081
OH	Slope of observed versus modeled	1.35 (1.21)[a]	1.16 (1.18)	1.12 (1.11)	1.12 (1.15)
	Intercept (10^6 cm^{-3})	0.00 (0.00)	0.00 (0.00)	0.00 (0.00)	0.00 (0.00)
	Median ratio	1.28 (1.14)	1.09 (1.13)	1.03 (1.05)	1.01 (1.04)
	Median percent difference (%)	25.0 (12.7)	11.0 (12.9)	3.3 (5.0)	1.2 (3.8)
	R^2	0.81 (0.78)	0.82 (0.79)	0.77 (0.75)	0.68 (0.62)
	Fraction of fOH within ±40%	0.63 (0.69)	0.68 (0.72)	0.80 (0.82)	0.77 (0.72)
HO_2	Slope of observed versus modeled	1.19 (1.00)	0.95 (1.02)	0.98 (0.94)	1.06 (0.97)
	Intercept (pptv)	−0.76 (−0.73)	0.05 (0.00)	−0.21 (+0.11)	−1.94 (−0.77)
	Median ratio	1.11 (0.96)	0.98 (1.01)	0.94 (0.94)	0.86 (0.88)
	Median percent difference (%)	10.4 (−3.6)	−2.0 (0.5)	−6.0 (−5.7)	−14.8 (−13.0)
	R^2	0.77 (0.72)	0.94 (0.91)	0.77 (0.72)	0.81 (0.81)
	Fraction of fHO_2 within ±40%	0.83 (0.72)	0.89 (0.90)	0.83 (0.82)	0.84 (0.90)
HO_2/OH	Median percent difference (%)	−15.2 (−24.0)	−14.9 (−12.1)	−13.9 (−18.1)	−25.9 (−29.8)
OH interference	Median (cm^{-3})	-8.7×10^3	9.1×10^4	8.8×10^4	8.5×10^4
	Standard deviation (cm^{-3})	2.7×10^5	2.4×10^5	2.7×10^5	3.4×10^5
	Percent within 5×10^5 cm^{-3} of 0.0	93	94	92	86

[a]Numbers for model constrained with TOGA HCHO in parentheses.

low levels of NO and VOCs (Figure S3; below 8 km). However, this ratio is still useful in assessing the agreement between observed and modeled OH and HO_2. As a function of altitude and latitude bands, the percent differences are generally within the ±40% band. This uncertainty band is actually somewhat lower because some calibration uncertainties are common to HO_2 and OH and thus cancel in the ratio, but the uncertainty band is still greater than ±30–35%. As shown in Figure 5, the percent differences tend to be positive (−10%–40%) near the ocean surface except in the polar regions, negative in the middle troposphere (−50–0%), and slightly less negative in the upper troposphere. The percent differences vary with both season and latitude.

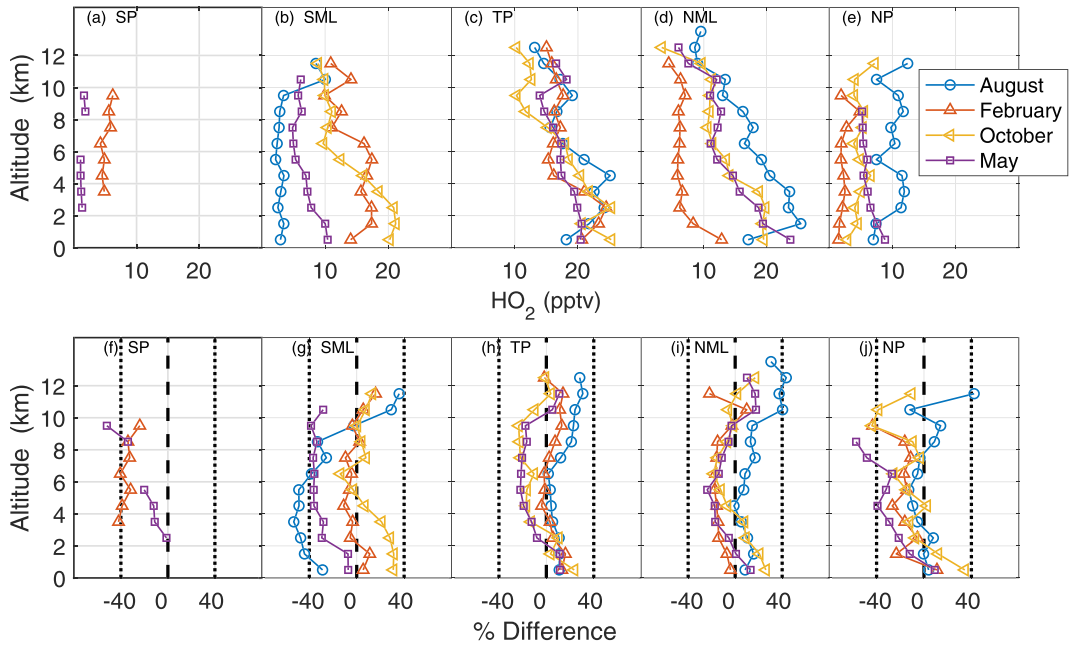

Figure 4. (a–e) Median midday altitude profiles of HO_2 and (f–j) the percent difference (equation (1)) between observed and modeled HO_2, as in Figure 3.

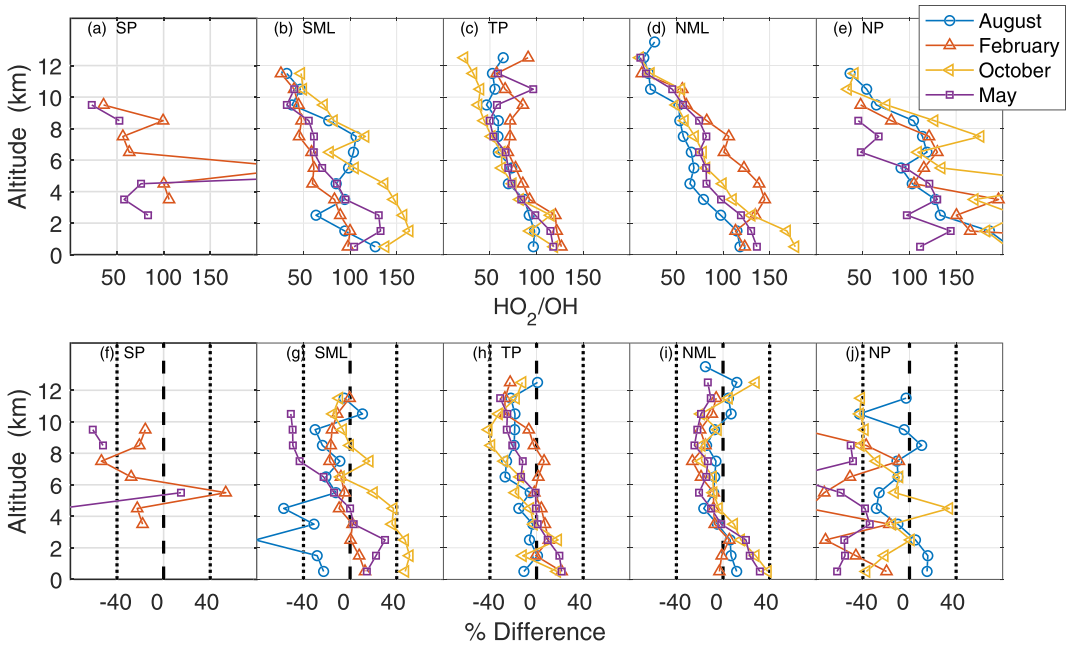

Figure 5. (a–e) Median midday altitude profiles of HO_2/OH and (f–j) the percent difference between observed and modeled HO_2/OH, as in Figure 3.

Despite the general agreement for observed and modeled OH and HO_2 to within measurement and model uncertainty, the persistence of modeled OH being less than observed in the middle-to-upper troposphere and modeled HO_2/OH being greater than observed as a function of altitude deserve a closer look.

5. Discussion

5.1. Comparison to Previous Studies

The level of agreement for observed and modeled OH and HO_2 is similar to that of other studies of OH and HO_2 in the free troposphere, particularly over oceans. Over the tropical Pacific Ocean during PEM-Tropics B, the slope of the OH modeled versus observed scatterplot was 1.26 for measurements below 6 km (Mauldin et al., 2001). These results are consistent with ATHOS measurements below 6 km from the same mission (Tan et al., 2001). Furthermore, the OH, HO_2, and HO_2/OH altitude trends observed during PEM-Tropics B are similar to those observed in ATom. However, in the lowest 2 km, the OH percent differences are ~5% for ATom but −27% for PEM-TB and HO_2 percent differences are ~12% for ATom and −12% for PEM-TB. As a result, the percent difference for the HO_2/OH ratio is ~10% greater for ATom than it is for PEM-TB. Model runs indicate that this difference is related to ATom peroxide and OVOC measurements made by instruments less susceptible to interferences.

For the HOOVER 2 study above 7 km over central Europe, observed and modeled OH and HO_2 were within uncertainties, with slopes of observed-to-modeled OH of 1.15 and HO_2 of 1.35, although the ratios of observed-to-modeled OH and HO_2 were within a few percent of 1 (Regelin et al., 2013). These results differ from ATom in the May-to-August northern midlatitudes above 7 km, for which the observed-to-modeled ratio was ~1.3 for OH and ~1.15 for HO_2. ATom and HOOVER 2 were different in two ways: the median NO in ATom was 1/3 that in HOOVER 2 and a greater number of constraining OH reactants and HO_x sources were measured in ATom, especially the OVOCs. Both of these factors could contribute to the differences between these two studies.

For the DC3 study around deep cumulus convection over the Central United States, median observed OH is equal to modeled up 6 km, becomes ~15% greater from 6 to 10 km, and then is ~20% less than modeled above 10 km (Brune et al., 2018). Median observed HO_2 goes from 40% greater than modeled near the surface to 20% less than modeled at 8 km and then becomes equal to the model above 9 km. In the lower and middle troposphere, the ATom and DC3 comparisons are similar. In the upper troposphere, the ATom HO_2

observed-to-modeled ratio is (10–20)% larger than for DC3 while ATom OH observed-to-modeled ratio is (10–40)% larger. Even when the DC3 data are filtered for NO < 0.1 ppbv and clear air and the ATom data are restricted to northern midlatitudes, the differences between DC3 and ATom remain despite the similar OVOC amounts for ATom and DC3 with these restrictions. For these restricted data sets, the abundances of the measured OVOCs for ATom are within a factor of 2 of those for DC3. Thus, it is not clear what is driving the differences in observed-to-modeled OH between DC3 and ATom if all measurements are actually within their stated uncertainties.

The generally good agreement and altitude trend in the free troposphere for ATom observed and modeled OH and HO_2 is different from the exceptional discrepancies that were described in section 1. For example, the altitude trends of the observed-to-modeled OH in ATom is opposite those observed in the August phase of ARCTAS (Olson et al., 2012). Without an analysis using the same model, the ATom comparisons provide no insight into the possible causes of these previous exceptions, whether it be the OH and HO_2 measurements, the model structure or chemistry, or the simultaneous measurements of other chemical species.

5.2. Upper Free Tropospheric OH and HO_2 Disagreement

The altitude trends in OH and HO_2 percent differences for the upper troposphere could be caused by errors in the ATHOS calibration, possible OH and HO_2 interferences, errors in the implementation of the model constraints, errors in the model chemistry, or errors in the measurements used to constrain the photochemical box model. We consider each of these in turn.

5.2.1. ATHOS Calibration

If the ATHOS calibration was the cause of the percent difference altitude trends, the calibration curves for OH and HO_2 would need to be, on average, ~35% different from the laboratory calibrations at the low-pressure end that corresponds to high altitude (Figure S1). Note that a higher calibration value will cause the calculated OH or HO_2 value to be lower. These values are just within the stated uncertainty of $\pm$**35** % ,**2σ** confidence, but for OH in ATom-1, the calibration at low pressure would need to be ~50% higher.

The instrument design and flow characteristics for ATHOS have changed little since 2000, so that it is reasonable to expect that the shape of the OH calibration curve as a function of pressure should be the same for all these missions. Four previous ATHOS OH calibrations have the same shape as the ATom calibration curve as a function of detection cell pressure to within $\pm$**14**%. It is also possible that the absolute calibration is in error. The ATHOS sensitivity can change from mission to mission because of changes in optics, detector sensitivity, or the number of passes of the laser through the detection cell. However, the ATom calibration is the highest of all calibrations at low cell pressure.

For HO_2 during ATom, a N_2 flow was added to the reagent NO addition system to improve the mixing of NO into the sample flow, and this addition did change the shape of the HO_2 calibration curve. As a result, only the comparison of the ATom OH calibration curve with those of previous missions is meaningful. Thus, we have more confidence in the OH calibration and its consistency than in the HO_2 calibration.

5.2.2. OH and HO_2 Interferences

An OH interference signal would make observed OH greater than it actually is. To explain the percent difference at high altitudes, it would need to be greater than 5×10^5 cm^{-3} (Figure 3). However, the median measured OH interference was less than 10^5 cm^{-3} for all ATom phases (Table 1), especially in the upper troposphere. Just above the ocean, 1% of the OH measurements exceed 10^6 cm^{-3} and some of these may actually prove to be an OH interference. However, we can say with confidence that the greater-than-modeled observed OH in the upper troposphere was not caused by an interference.

Similarly, an HO_2 interference signal would make observed HO_2 greater than it actually is. In the remote, relatively clean troposphere, the low amounts of larger alkenes, aromatics, and cyclic alkanes would cause negligible HO_2 interference signals even if enough reagent NO was being added to completely convert HO_2 to OH. Indeed, when accounting for the differences in conversion efficiency, the median HO_2 derived from 0.5-sccm NO flow is only 5% lower than that from the 7.0-sccm flow, well within the uncertainty of the HO_2 conversion efficiency. Thus, an HO_2 interference cannot cause the larger percent difference between observed and modeled HO_2.

5.2.3. Model Treatment Error

Model parameters could cause the discrepancies between the observed and modeled OH and HO_2. The most important of these are filling in missing data for the constraining measurements and the integration time. First, filtering the data for times when all the constraining measurements were available reduced the interpolated measurement data set used to constrain the model to 67% of the initial 1-min time points for ATom 1. The comparison of the observed and filtered modeled OH and HO_2 did not change any of the comparison statistics by more than 4%. Thus, using the interpolated measurement data set to constrain the model cannot account for the high-altitude discrepancy. Second, changing integration time from one to five days changed median OH and HO_2 by less than 0.1%, while the maximum difference at any one 1-min point was 7% for one day compared to three days and less than 0.1% for five days compared to three days. Changing the dilution time between half and five days changed OH and HO_2 by less than 1%. Altering these model treatments did not relieve the OH and HO_2 discrepancies in the upper troposphere.

5.2.4. Chemical Mechanism

For OH observations exceeding modeled values in the upper troposphere, if there is an error in the model chemistry, it could be either a missing OH source or an overestimated OH sink. The OH sinks involve well-known reactions with CO, CH_4, HOOH, CH_3OOH, CH_3CHO, HCHO, and other VOCs. The peroxides and aldehydes are also HO_x sources. The 2σ uncertainty of the total OH sink is less than 15%. It is difficult to imagine that the total OH sink is ~1.35 times smaller than modeled, which is the amount necessary to explain difference between observed and modeled OH and HO_2/OH at higher altitudes.

The primary known halogen for the upper troposphere is bromine. Reactions between bromine species and HO_x mainly cycle HO_x between OH and HO_2. Above 7-km altitude, the median of 1-min averages for BrO was 0.07 pptv and the maximum was 0.38 pptv. The model run augmented with halogen chemistry and constrained by the measured BrO changed OH and HO_2 by less than 2%, with lower values above 8-km altitude. With such low BrO values, OH and HO_2 are essentially unaffected by bromine chemistry in the free troposphere for ATom.

HO_2 uptake could provide another loss of HO_x and also alter the balance between OH and HO_2. The gas-phase HO_x loss rates are relatively low in this remote air so that HO_2 uptake on aerosol particles could be important. Modeled HO_2 is decreased −5% below 2 km, −2% at 2 km, and slowly became more negative to −3% above 10 km. Modeled OH is decreased ~−1% below 4 km, and then slowly became more negative to −3% above 10 km. Eighty percent of the HO_2 decreases are less than 5% while 90% of OH decreases are less than 5%. If a HO_2 uptake coefficient of 1.0 is used, the model decrease for HO_2 is several tens of percent. As a result, the addition of HO_2 uptake in the model tends to increase the percent difference between observed and modeled OH and HO_2. Thus, as was found in two previous studies (Brune et al., 2018; Olson et al., 2006), adding substantial HO_2 uptake is inconsistent with observed OH and HO_2.

The tropospheric levels of pollutants such as HCHO, CO, O_3, and the HO_x production rate tended to be higher over the Atlantic than over the Pacific. As a result, HO_x tends to be greater over the Atlantic than over the Pacific, especially in the tropics. If the chemical mechanism is the cause of the HO_x observed-to-modeled discrepancy, then its influence might appear in the percent differences between observed and modeled OH and HO_2 over the two oceans. However, the altitude profiles of the OH and HO_2 percent differences are essentially identical over the two oceans, indicating that the chemical mechanism is able to account for the difference in pollution levels over the two oceans.

HO_x production and loss consists primarily of radical-radical reactions for loss and photolysis of ozone or OVOCs for production (Figure S2). To cause the discrepancy between observed and modeled HO_x in the upper troposphere during August (ATom-1), the HO_x production rate would need to be ~1.35 times larger than modeled, which translates into the need for an additional HO_x production rate of roughly 6×10^4 cm^{-3} s^{-1} for altitudes above 10 km (Figure S4). We do not know the identity of this possible additional HO_x production but if we assume that it is the photolysis of a "formaldehyde-like" chemical species, the amount of formaldehyde-like chemical would need to be on average 50 pptv above 10-km altitude. While this amount is not large, it is ~60% of the measured formaldehyde. On the other hand, it seems unlikely that some additional unknown HO_x source existed for August in quantities much greater than those in the other three seasons.

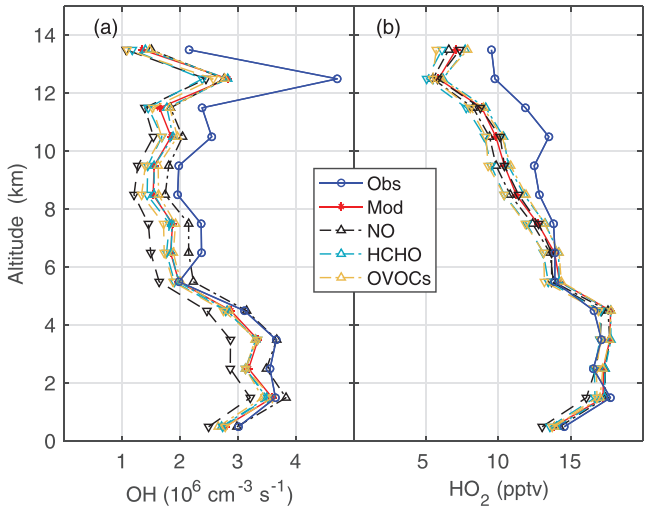

Figure 6. Sensitivity of (a) OH and (b) HO_2 as a function of altitude to the uncertainty in NO (black), HCHO by NASA ISAF (aqua), and OVOCs by TOGA and CIT-CIMS (gold) for ATom-1. Median values are found over each 0.5-km band for modeled (red stars) and observed (blue circles) OH and HO_2. Upright triangles indicate measured value plus the 2σ uncertainty and inverted triangles indicate measured value minus the 2σ uncertainty.

5.2.5. Simultaneous Measurements

It is possible that one or more of the simultaneous measurements that are used to constrain the box model are responsible for the larger percent difference at high altitudes. NO and OVOCs are particularly important. NO cycles HO_2 into OH, affecting mainly OH, while OVOCs cycle OH into HO_2 and are a HO_x source. The most important OVOCs are formaldehyde, acetaldehyde, hydrogen peroxide, methylhydroperoxide, and peroxyacetic acid (Figure S2). For ATom-1, when NO, HCHO, or the group of other OVOCs are changed one at a time to the limits of their stated uncertainties at 2σ confidence, modeled OH and HO_2 are still less than the observed for most altitudes (Figure 6). In all cases, setting the abundances to their upper limits improves the agreement between the observed and modeled OH and HO_2.

For ATom-2, ATom-3, and ATom-4, observed and modeled OH agreed with the model to within the model uncertainties, except for ATom-4 above 6-km altitude (Figures S5–S7). On the other hand, observed HO_2 is generally not within the model range, being lower than the model from 4 to 10 km and greater than or equal to the model below 2 km and above 10 km. This lack of consistency among missions suggests either seasonal changes in some unknown chemistry or changes in some instruments' performance.

An example of changing instrument performance is formaldehyde (Figure 7), which was measured by two instruments, TOGA and ISAF (Table S2). When the ratio of TOGA HCHO to ISAF HCHO is plotted in order of when HCHO was measured, a downward trend emerges. The black solid line in Figure 7 is generally within the combined uncertainties at **2σ** confidence, the ratio shifts from about 2 at the beginning to ½ at the end. Which instruments are changing is not known. Interestingly, constraining the model with TOGA HCHO somewhat improves the observed-to-modeled agreement for both OH and HO_2 for ATom-1 (Table 1 (parentheses) and Figures S8 and S9). It is certainly possible that the performance of instruments that measure other chemical species also changed in unknown ways because there is no way to check chemical species that were measured by only one instrument or that cannot be modeled.

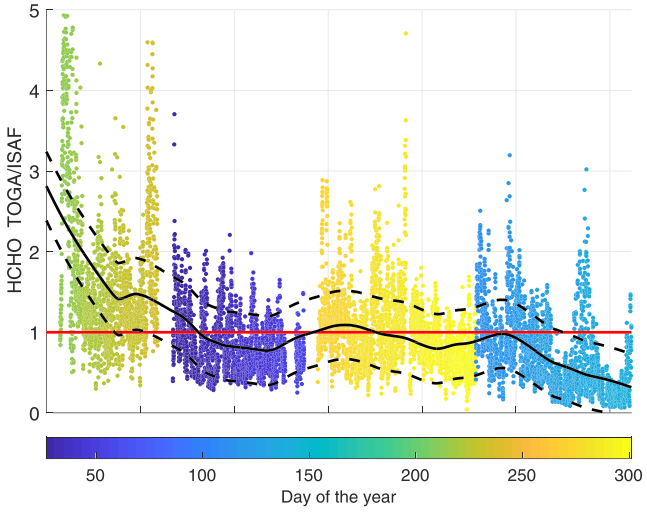

Figure 7. Ratio of TOGA-to-ISAF formaldehyde data averaged into 2-min bins for ATom-1, ATom-2, ATom-3, and ATom-4 in the order they were undertaken. The median ratio (black line) and ±the combined instrument uncertainty at ±2σ confidence (black dashed lines) are averaged over ~8 flights and compared to the 1:1 line (red) for which the two measurements would be in perfect agreement.

6. Conclusions

Much has been learned about atmospheric oxidation by OH in the remote, relatively clean troposphere in the past 48 years since Levy published his paper. There are more HO_x sources than previously thought, so that OH and HO_2 do not decrease with increasing altitude and latitude as much as that calculated in Logan et al. (1981). While the earliest airborne OH measurements indicated missing OH sources in the upper troposphere, it was not until reliable measurements of NO, HCHO, H_2O_2, VOCs, and OVOCs were made that models, constrained with these measurements, could consistently reproduce OH and HO_2 measurements to within the measurement and model uncertainties. ATom has now extended OH and HO_2 measurements in relatively clean conditions to vast previously undersampled swaths of the remote free troposphere over oceans in each season.

Despite some apparent seasonal differences that will need more examination in a future paper, the altitude-dependent discrepancies between median observed and modeled OH and HO_2 persist in most latitude bands and seasons. These altitude trends, while evident, generally reside within combined uncertainty ranges of the model and the measurement at the 2σ confidence level. The OH and HO_2 altitude trends and their changes with latitude band and season imply that some aspects of either the oxidation chemistry or instrument performance are not completely understood, especially in the upper troposphere. However, these results do not disprove the hypothesis that atmospheric oxidation chemistry of OH and HO_2 in the remote, relatively clean free troposphere is well understood.

Concerns have been expressed that previous airborne ATHOS OH and HO_2 measurements were compromised because ATHOS did not employ the interference mitigation methods that were used for ATom. The ATHOS measurements of the OH and HO_2 interferences demonstrate that these interferences are negligible for the environments encountered in ATom. Thus, while these interferences may be a problem for previous measurements of OH and HO_2 in air that contains substantial amounts of alkenes, aromatics, and ozone, the ATHOS OH and HO_2 measurements are likely unbiased by such artifacts for the several previous missions in the relatively clean free troposphere.

Where do we go from here?

First, individual flights need to be examined in detail. On several flights, the relationship between observed and modeled OH and HO_2 changes from the model being higher to the measurement being higher for the same altitudes. Analysis of discrepancies such as these may uncover errors in the measurements or model chemistry that are being masked by the analysis of median OH and HO_2 in this paper.

Second, the existing data set of airborne HO_x needs to be unified so that it can be used test the oxidation chemistry in chemical transport models and its response to human-caused changes in atmospheric composition. Right now, it is not known if differences in the HO_x observation and model relationship from mission to mission are due to changes in the measuring instruments or changes in the model. Using a single model for previous aircraft campaigns that included OH and HO_2 measurements will enable an assessment of measurement consistency and accuracy.

Third, the accuracy, precision, and consistency of the measurements must be improved in order to test atmospheric oxidation chemistry at a level that is more useful for chemical transport models and analyses of oxidation capacity trends. The limit of detection for essential constraining measurements, such as NO, needs to be lowered substantially. Currently, measurement uncertainty and possible unknown errors and variability appear to be the more likely cause of the differences between observed and modeled OH and HO_2 than unknown chemistry or incorrect reaction rate coefficients.

Fourth, the accuracy of the model chemistry must also be improved. Uncertainties must be reduced by roughly a factor of 2 for OH, HO_2 and for critical reaction rate coefficients and their pressure and temperature dependencies for reactions such as $\mathbf{HO_2 + NO \rightarrow OH + NO_2}$ and $\mathbf{OH + NO_2 + M \rightarrow HNO_3 + M}$, and for the photolysis frequencies for O_3, NO_2, and HCHO (Christian et al., 2017).

For the past two decades, measurements and models of OH and HO_2 have gone through cycles of field deployment, discovery, re-evaluation, and improvement. All the while, the understanding of atmospheric oxidation in the free troposphere has expanded and confidence in it has grown. At some time, model

atmospheric chemistry mechanisms may be tested well enough that OH and HO_2 measurements will no longer be a critical component of field deployments, but now is not that time.

Data and Model Availability

The data and model used in this paper are publicly available:

- data: https://doi.org/10.3334/ORNLDAAC/1581
- model framework: https://sites.google.com/site/wolfegm/models
- MCMv331 chemical mechanism: http://mcm.leeds.ac.uk/MCM/

Author Contribution

D.O.M., W.H.B., and A.B.T. made the OH and HO_2 measurements, performed the model runs, analyzed the data, and wrote the initial draft of the manuscript. G.M.W. provided support the F0AM model framework. W.H.B., D.O.M., A.B.T., H.M.A., E.C.A., D.R.B., T.P.B., R.C., J.D.C., B.C.D., G.S.D., J.P.D., J.W.E., S.R.H., T.F.H., R.A.H., E.J.H., R.S.H., M.J.K., K.M., F.L.M., J.M.N., J.A.N., J.P., T.B.R., J.M.S., C.S., A.P.T., C.T., K. U., P.R.V., P.O.W., and G.M.W. provided ATom measurements used for the modeling and edits for the manuscript.

Competing Interests

The authors declare no financial or affiliation conflicts of interest.

Funding

This study was supported by the NASA grant NNX15AG59A. This material is based upon work supported by the National Center for Atmospheric Research, which is a major facility sponsored by the National Science Foundation under cooperative agreement 1852977. M.J.K. was supported by NSF fellowship 1524860 for the first year of this study.

Acknowledgments
The authors thank the NASA ATom management team, pilots, logistical support team, aircraft operations team, and fellow scientists.

References

Adhikary, B., Carmichael, G. R., Kulkarni, S., Weil, C., Tang, Y., D'Allural, A., et al. (2010). A regional scale modeling analysis of aerosol and trace gas distributions over the eastern Pacific during the INTEX-B field campaign. *Atmospheric Chemistry and Physics*, *10*, 2091–2115. https://doi.org/10.5194/acp-10-2091-2010

Assaf, E., Sheps, L., Whalley, L., Heard, D., Tomas, A., Schoemaecker, C., & Fittschen, C. (2017). The reaction between CH_3O_2 and OH radicals: Product yields and atmospheric implications. *Environmental Science & Technology*, *51*(4), 2170–2177. https://doi.org/10.1021/acs.est.6b06265

Blitz, M. A., Heard, D. E., Pilling, M. J., Arnold, S. R., & Chipperfield, M. P. (2004). Pressure and temperature-dependent quantum yields for the photodissociation of acetone between 279 and 327.5 nm. *Geophysical Research Letters*, *31*, L06111. https://doi.org/10.1029/2003GL018793

Brune, W. H., Faloona, I. C., Tan, D., Weinheimer, A. J., Campos, T., Ridley, B. A., et al. (1998). Airborne in situ OH and HO_2 observations in cloud-free troposphere and lower stratosphere during SUCCESS. *Geophysical Research Letters*, *25*, 1701–1704.

Brune, W. H., Ren, X., Zhang, L., Mao, J., Miller, D. O., Anderson, B. E., et al. (2018). Atmospheric oxidation in the presence of clouds during the Deep Convective Clouds and Chemistry (DC3) study. *Atmospheric Chemistry and Physics*, *18*, 14,493–14,510. https://doi.org/10.5194/acp-18-14493-2018

Cantrell, C. A., Edwards, G. D., Stephens, S., Mauldin, L., Kosciuch, E., & Zondlo, M. (2003a). Peroxy radical observations using chemical ionization mass spectrometry during TOPSE. *Journal of Geophysical Research*, *108*(D6), 8371. https://doi.org/10.1029/2002JD002715

Cantrell, C. A., Edwards, G. D., Stephens, S., Mauldin, R. L., Zondlo, M. A., Kosciuch, E., et al. (2003b). Peroxy radical behavior during the Transport and Chemical Evolution over the Pacific (TRACE-P) campaign as measured aboard the NASA P-3B aircraft. *Journal of Geophysical Research*, *108*(D20), 8797. https://doi.org/10.1029/2003JD003674

Cantrell, C. A., Mauldin, L., Zondlo, M., Eisele, F., Kosciuch, E., Shetter, R., et al. (2003). Steady state free radical budgets and ozone photochemistry during TOPSE. *Journal of Geophysical Research*, *108*(D4), 8361. https://doi.org/10.1029/2002JD002198

Chen, G., Davis, D., Crawford, J., Hekies, B., O'Sullivan, D., Lee, M., et al. (2001). An assessment of the HO_x chemistry in the tropical Pacific boundary layer: Comparison of model simulations with observations recorded during PEM tropics A. *Journal of Atmospheric Chemistry*, *38*, 317–344. https://doi.org/10.1023/A:1006402626288

Chen, S., Brune, W. H., Oluwole, O. O., Kolb, C. E., Bacon, F., Li, G. Y., & Rabitz, H. (2012). Global sensitivity analysis of the regional atmospheric chemical mechanism: An application of random sampling-high dimensional model representation to urban oxidation chemistry. *Environmental Science & Technology*, *46*, 11,162–11,170. https://doi.org/10.1021/es301565w

Christian, K. E., Brune, W. H., & Mao, J. Q. (2017). Global sensitivity analysis of the GEOS-Chem chemical transport model: ozone and hydrogen oxides during ARCTAS (2008). *Atmospheric Chemistry and Physics*, *17*, 3769–3784.

Davis, D., Grodzinsk, G., Chen, G., Crawford, J., Eisele, F., Mauldin, L., et al. (2001). Marine latitude/altitude OH distributions: Comparison of Pacific Ocean observations with models. *Journal of Geophysical Research*, *106*, 32,691–32,707. https://doi.org/10.1029/2001JD900141

Faloona, I. C., Tan, D., Lesher, R. L., Hazen, N. L., Frame, C. L., Simpas, J. B., et al. (2004). A laser-induced fluorescence instrument for detecting tropospheric OH and HO_2: Characteristics and calibration. *Journal of Atmospheric Chemistry*, *47*, 139–167.

Feiner, P. A., Brune, W. H., Miller, D. O., Zhang, L., Cohen, R. C., Romer, P. S., et al. (2016). Testing atmospheric oxidation in an Alabama forest. *Journal of the Atmospheric Sciences*, *73*(12), 4699–4710. https://doi.org/10.1175/JAS-D-16-0044.1

Fuchs, H., Bohn, B., Hofzumahaus, A., Holland, F., Lu, K. D., Nehr, S., et al. (2011). Detection of HO_2 by laser-induced fluorescence: Calibration and interferences from RO_2 radicals. *Atmospheric Measurement Techniques*, *4*, 1209–1225.

Hard, T. M., O'Brian, R. J., Chan, C. Y., & Mehrabzadeh, A. A. (1984). Tropospheric free radical determination by FAGE. *Environmental Science & Technology*, *18*, 768–777.

Jaeglé, L., Jacob, D., Brune, W., Faloona, I., Tan, D., Heikes, B., et al. (2000). Photochemistry of HO_x in the upper troposphere at northern latitudes. *Journal of Geophysical Research*, *105*(D3), 3877–3892. https://doi.org/10.1029/1999JD901016

Jaeglé, L., Jacob, D. J., Brune, W. H., Tan, D., Faloona, I. C., Weinheimer, A. J., et al. (1998). Sources of HO_x and production of ozone in the upper troposphere over the United States. *Geophysical Research Letters*, *25*, 1709–1712.

Jenkin, M. E., Saunders, S. M., Wagner, V., & Pilling, M. J. (2003). Protocol for the development of the Master Chemical Mechanism, MCM v3 (Part B): Tropospheric degradation of aromatic volatile organic compounds. *Atmospheric Chemistry and Physics*, *3*, 181–193. https://doi.org/10.5194/acp-3-181-2003

Levy, H. II (1971). Normal atmosphere: Large radical and formaldehyde concentrations predicted. *Science*, *173*(3992), 141–143. https://doi.org/10.1126/science.173.3992.141

Logan, J. A., Prather, M. J., Wofsy, S. C., & McElroy, M. B. (1981). Tropospheric chemistry: A global perspective. *Journal of Geophysical Research*, *86*(C8), 7210–7254. https://doi.org/10.1029/JC086iC08p07210

Mao, J., Jacob, D. J., Evans, M. J., Olson, J. R., Ren, X., Brune, W. H., et al. (2010). Chemistry of hydrogen oxide radicals (HO_x) in the Arctic troposphere in spring. *Atmospheric Chemistry and Physics*, *10*, 5823–5838.

Mao, J., Ren, X., Zhang, L., Van Duin, D. M., Cohen, R. C., Park, J.-H., et al. (2012). Insights into hydroxyl measurements and atmospheric oxidation in a California forest. *Atmospheric Chemistry and Physics*, *12*, 8009–8020. https://doi.org/10.5194/acp-10-5823-2010

Martinez, M., Harder, H., Kubistin, D., Rudolf, M., Bozem, H., Eerdekens, G., et al. (2010). Hydroxyl radicals in the tropical troposphere over the Suriname rainforest: Airborne measurements. *Atmospheric Chemistry and Physics*, *10*, 3759–3773. https://doi.org/10.5194/acp-10-3759-2010

Mauldin, R. L. III, Eisele, F. L., Cantrell, C. A., Kosciuch, E., Ridley, B. A., Lefer, B., et al. (2001). Measurements of OH aboard the NASA P-3 during PEM Tropics B. *Journal of Geophysical Research*, *106*(D23), 32,657–32,666. https://doi.org/10.1029/2000JD900832

Mauldin, R. L. III, Tanner, D. J., & Eisele, F. L. (1999). Measurements of OH during PEM-Tropics A. *Journal of Geophysical Research*, *104*(D5), 5817–5827. https://doi.org/10.1029/98JD02305

Mauldin, R. L. III, Tanner, D. J., Frost, G. J., Chen, G., Prevot, A. S. H., Davis, D. D., & Eisele, F. L. (1998). OH measurements during ACE-1: Observations and model comparisons. *Journal of Geophysical Research*, *103*(D13), 16,713–16,729. https://doi.org/10.1029/98JD00882

Olson, J. R., Crawford, J. H., Brune, W., Mao, J., Ren, X., Fried, A., et al. (2012). An analysis of fast photochemistry over high northern latitudes during spring and summer using in-situ observations from ARCTAS and TOPSE. *Atmospheric Chemistry and Physics*, *12*, 6799–6825. https://doi.org/10.5194/acp-12-6799-2012

Olson, J. R., Crawford, J. H., Chen, G., Brune, W. H., Faloona, I. C., Tan, D., et al. (2006). A reevaluation of airborne HO_x observations from NASA field campaigns. *Journal of Geophysical Research*, *111*, D10301. https://doi.org/10.1029/2005JD006617

Olson, J. R., Crawford, J. H., Chen, G., Fried, A., Evans, M. J., Jordan, C. E., et al. (2004). Testing fast photochemical theory during TRACE-P based on measurements of OH, HO_2, and CH_2O. *Journal of Geophysical Research*, *109*, D15S10. https://doi.org/10.1029/2003JD004278

Regelin, E., Harder, H., Martinez, M., Kubistin, D., Tatum Ernest, C., Bozem, H., et al. (2013). HO_x measurements in the summertime upper troposphere over Europe: A comparison of observations to a box model and a 3-D model. *Atmospheric Chemistry and Physics*, *13*, 10,703–10,720. https://doi.org/10.5194/acp-13-10703-2013

Ren, X., Mao, J., Brune, W. H., Cantrell, C. A., Mauldin, R. L., Hornbrook, R. S., et al. (2012). Airborne intercomparison of HO_x measurements using laser-induced fluorescence and chemical ionization mass spectrometry during ARCTAS. *Atmospheric Measurement Techniques*, *5*, 2025–2037. https://doi.org/10.5194/amt-5-2025-2012

Ren, X. R., Olson, J. R., Crawford, J. H., Brune, W. H., Mao, J. Q., Long, R. B., et al. (2008). HO_x chemistry during INTEX-A 2004: Observation, model calculation, and comparison with previous studies. *Journal of Geophysical Research*, *113*, D05310. https://doi.org/10.1029/2007JD009166

Saunders, S. M., Jenkin, M. E., Derwent, R. G., & Pilling, M. J. (2003). Protocol for the development of the Master Chemical Mechanism, MCM v3 (Part A): Tropospheric degradation of non-aromatic volatile organic compounds. *Atmospheric Chemistry and Physics*, *3*, 161–180. https://doi.org/10.5194/acp-3-161-2003

Stevens, P. S., Mather, J. H., & Brune, W. H. (1994). Measurement of OH and HO2 by laser-induced fluorescence at low pressure, *Journal of Geophysical Research*, *99*, 3543–3557.

Stone, D., Evans, M. J., Commane, R., Ingham, T., Floquet, C. F. A., McQuaid, J. B., et al. (2010). HO_x observations over West Africa during AMMA: Impact of isoprene and NO_x. *Atmospheric Chemistry and Physics*, *10*, 9415–9429. https://doi.org/10.5194/acp-10-9415-2010

Stone, D., Evans, M. J., Edwards, P. M., Commane, R., Ingham, T., Rickard, A. R., et al. (2011). Isoprene oxidation mechanisms: measurements and modelling of OH and HO_2 over a South-East Asian tropical rainforest during the OP3 field campaign. *Atmospheric Chemistry and Physics*, *11*, 6749–6771. https://doi.org/10.5194/acp-11-6749-2011

Stone, D., Evans, M. J., Walker, H. M., Ingham, T., Vaughan, S., Ouyang, B., et al. (2014). Radical chemistry at night: Comparisons between observed and modelled HO_x, NO_3 and N_2O_5 during the RONOCO project. *Atmospheric Chemistry and Physics*, *14*, 1299–1321. https://doi.org/10.5194/acp-14-1299-2014

Stone, D., Sherwen, T., Evans, M. J., Vaughan, S., Ingham, T., Whalley, L. K., et al. (2018). Impacts of bromine and iodine chemistry on tropospheric OH and HO_2: Comparing observations with box and global model perspectives. *Atmospheric Chemistry and Physics*, *18*, 3541–3561. https://doi.org/10.5194/acp-18-3541-2018

Stone, D., Whalley, L. K., & Heard, D. E. (2014). Tropospheric OH and HO_2 radicals: Field measurements and model comparisons. *Chemical Society Reviews*, *41*, 6348–6404.

Tan, D., Faloona, I., Brune, W. H., Weinheimer, A., Campos, T., Ridley, B., et al. (1998). In situ measurements of HO_x in aircraft exhaust plumes and contrails during SUCCESS. *Geophysical Research Letters*, *25*(10), 1721–1724. https://doi.org/10.1029/98GL00117

Tan, D., Faloona, I., Simpas, J. B., Brune, W., Olson, J., Crawford, J., et al. (2001). OH and HO_2 in the remote tropical Pacific: Results from PEM-Tropics B. *Journal of Geophysical Research*, *106*(D23), 32,667–32,681. https://doi.org/10.1029/2001JD900002

Thompson, A. M., & Stewart, R. W. (1991). Effect of chemical kinetics uncertainties on calculated constituents in a tropospheric photochemical model. *Journal of Geophysical Research*, *96*(D7), 13,089–13,108. https://doi.org/10.1029/91JD01056

Wennberg, P. O., Hanisco, T. F., Jaegle, L., Jaconb, D. J., Hintsa, E. J., Lanzendorf, E. J., et al. (1998). Hydrogen radicals, nitrogen radicals, and the production of O_3 in the upper troposphere. *Science*, *279*(5347), 49–53. https://doi.org/10.1126/science.279.5347.49

Whalley, L. K., Blitz, M. A., Desservettaz, M., Seakins, P. W., & Heard, D. E. (2013). Reporting the sensitivity of laser-induced fluorescence instruments used for HO_2 detection to an interference from RO_2 radicals and introducing a novel approach that enables HO_2 and certain RO_2 types to be selectively measured. *Atmospheric Measurement Techniques*, *6*, 3425–3440. https://doi.org/10.5194/amt-6-3425-2013

Wofsy, S. C., Afshar, S., Allen, H. M., Apel, E., Asher, E. C., Barletta, B., et al. (2018). *ATom: Merged Atmospheric Chemistry, Trace Gases, and Aerosols*. Oak Ridge, Tennessee. USA. USA: ORNL DAAC. https://doi.org/10.3334/ORNLDAAC/1581

Wolfe, G. M., Marvin, M. R., Roberts, S. J., Travis, K. R., & Liao, J. (2016). The Framework for 0-D Atmospheric Modeling (F0AM) v3.1. *Geoscientific Model Development*, *9*, 3309–3319. https://doi.org/10.5194/gmd-9-3309-2016

York, D., Evensen, N., Martinez, M., & Delgado, J. (2004). Unified equations for the slope, intercept, and standard errors of the best straight line. *American Journal of Physics*, *72*, 367–375. https://doi.org/10.1119/1.1632486

References From the Supporting Information

Apel, E. C., Hornbrook, R. S., Hills, A. J., Blake, N. J., Barth, M. C., Weinheimer, A., et al. (2015). Upper tropospheric ozone production from lightning NOximpacted convection: Smoke ingestion case study from the DC3 campaign. *Journal of Geophysical Research: Atmospheres*, *120*, 2505–2523. https://doi.org/10.1002/2014JD022121

Cazorla, M., Wolfe, G. M., Bailey, S. A., Swanson, A. K., Arkinson, H. L., & Hanisco, T. F. (2015). A new airborne laserinduced fluorescence instrument for in situ detection of formaldehyde throughout the troposphere and lower stratosphere. *Atmospheric Measurement Techniques*, *8*, 541–552. https://doi.org/19410.5194/amt85412015

Chan, K. R., DeanDay, J., Bowen, S. W., & Bui, T. P. (1998). Turbulence measurements by the DC8 meteorological measurement system. *Geophysical Research Letters*, *25*, 1355–1358. https://doi.org/10.1029/97GL03590

Chen, H., Karion, A., Rella, C. W., Winderlich, J., Gerbig, C., Filges, A., & Tans, P. P. (2013). Accurate measurements of carbon monoxide in humid air using the cavity ringdown spectroscopy (CRDS) technique. *Atmospheric Measurement Techniques*, *6*, 1031–1040. https://doi.org/10.5194/amt610312013

Colman, J. J., Swanson, A. L., Meinardi, S., Sive, B. C., Blake, D. R., & Rowland, F. S. (2001). Description of the analysis of a wide range of volatile organic compounds in whole air samples collected during PEMTropics A and B. *Analytical Chemistry*, *73*(15), 3723–3731. https://doi.org/10.1021/ac010027g

Crounse, J. D., McKinney, K. A., Kwan, A. J., & Wennberg, P. O. (2006). Measurement of gasphase hydroperoxides by chemical ionization mass spectrometry. *Analytical Chemistry*, *78*(19), 6726–6732. https://doi.org/10.1021/ac0604235

Diskin, G. S., J. R. Podolske, G. W. Sachse, and T. A. Slate (2003). Open path airborne tunable diode laser hygrometer. 4817, 196, International Society for Optics and Photonics. https://doi.org/22510.1117/12.453736

Neuman, J. A., Trainer, M., Brown, S. S., Min, K.E., Nowak, J. B., Parrish, D. D., & Veres, P. R. (2016). HONO emission and production determined from airborne measurements over the Southeast U.S. *Journal of Geophysical Research: Atmospheres*, *121*, 9237–9250. https://doi.org/10.1002/2016JD025197

Ryerson, T. B., Williams, E. J., & Fehsenfeld, F. C. (2000). An efficient photolysis system for fast response NO_2 measurements. *Journal of Geophysical Research*, *105*, 26,447–26,461. https://doi.org/10.1029/2000JD900389

Santoni, G. W., Daube, B. C., Kort, E. A., Jimenez, R., Park, S., Pittman, J. V., & Wofsy, S. C. (2014). Evaluation of the airborne quantum cascade laser spectrometer (QCLS) measurements of the carbon and greenhouse gas suiteCO_2, CH_4, N_2O, and COduring the CalNex and HIPPO campaigns. *Atmospheric Measurement Techniques*, *7*, 1509–1526. https://doi.org/10.5194/amt715092014

Shetter, R. E., & Mueller, M. (1999). Photolysis frequency measurements using actinic flux spectroradiometry during the PEMTropics mission: Instrumentation description and some results. *Journal of Geophysical Research*, *104*, 5647–5661. https://doi.org/10.1029/98JD01381